

# Collective Properties of Low-lying Octupole Excitations in ${}^{208}_{82}\text{Pb}_{126}$ , ${}^{60}_{20}\text{Ca}_{40}$ and ${}^{28}_8\text{O}_{20}$

X.R. Zhou <sup>a,b</sup>, E.G. Zhao <sup>a,b,d</sup>, B.G. Dong <sup>c</sup>, X.Z. Zhang <sup>c</sup>,  
G.L. Long <sup>a,d</sup>

<sup>a</sup>*Department of Physics, Tsinghua University, Beijing 100084, P.R. China*

<sup>b</sup>*Institute of Theoretical Physics, Chinese Academy of Sciences, Beijing 100080,  
P.R. China*

<sup>c</sup>*China Institute of Atomic Energy, P.O. Box 275, Beijing 102431, P.R. China*

<sup>d</sup>*Center of Theoretical Physics, National Laboratory of Heavy Ion Accelerator,  
Lanzhou 730000, P.R. China*

---

## Abstract

The octupole strengths of three nuclei:  $\beta$ -stable nucleus  ${}^{208}_{82}\text{Pb}_{126}$ , neutron skin nucleus  ${}^{60}_{20}\text{Ca}_{40}$  and neutron drip line nucleus  ${}^{28}_8\text{O}_{20}$  are studied by using the self-consistent Hartree-Fock calculation with the random phase approximation. The collective properties of low-lying excitations are analyzed by particle-vibration coupling. The results show that there is the coexistence of the collective excitations and the decoupled strong continuum strength near the threshold in the lowest isoscalar states in  ${}^{60}_{20}\text{Ca}_{40}$  and  ${}^{28}_8\text{O}_{20}$ . For these three nuclei, both the low-lying isoscalar states and giant isoscalar resonance carry isovector strength. The ratio  $B(\text{IV})/B(\text{IS})$  is checked and it is found that, for  ${}^{208}_{82}\text{Pb}_{126}$ , the ratio is equal to  $(\frac{N-Z}{A})^2$  in good accuracy, while for  ${}^{60}_{20}\text{Ca}_{40}$  and  ${}^{28}_8\text{O}_{20}$ , the ratios are much larger than  $(\frac{N-Z}{A})^2$ . The study shows that the enhancement of the ratio is due to the excess neutrons that have small binding energies in  ${}^{60}_{20}\text{Ca}_{40}$  and  ${}^{28}_8\text{O}_{20}$ .

*PACS:* 21.10.Re, 21.60.Ev, 21.60.Jz, 27.30.+t

*Keywords:* Neutron drip line nuclei; Collective excitations; Particle-vibration coupling; transition current; transition density

---

## 1 Introduction

Various exotic properties are expected for nuclei far from  $\beta$ -stability. The collective properties of neutron drip line nuclei are especially interesting, because neutrons with small binding energies show a unique response to external fields.

In the Ref. [1–7], monopole, dipole and quadrupole isoscalar (IS) and isovector (IV) giant resonances in stable and drip line, particularly neutron drip line nuclei, were studied by using the self-consistent Hartree-Fock (HF) calculation plus random phase approximation (RPA) with Skyrme interaction, and both the IS and IV correlations were taken into account simultaneously. It was found that for both  $\beta$ -stable and drip line nuclei the giant resonances can be well described by the collective model [8,9]. For neutron drip line nuclei, however, there is appreciable amount of low-lying strengths just above threshold and these low-lying strengths are nearly pure neutron unperturbed excitations. For example, in Ref[4], the quadrupole strength of the neutron drip line nucleus  ${}^{28}_8\text{O}_{20}$  was analyzed and it was pointed out that there exists a so-called threshold strength, which is not of collective character and comes from the excitations of excess neutrons with small binding energies. In a recent publication [11], the low-lying octupole excitation of the neutron skin nucleus  ${}^{60}_{20}\text{Ca}_{40}$  was studied and it was pointed out the low-lying ( $\Delta N = 1$ ) IS octupole states appear as collective excitation and are shifted down to very low energy region, due to the disappearance of the N=50 magic number. Low-lying octupole excitations usually consist of transitions from occupied states to bound states, resonance states and nonresonance states. In this paper, we make a detailed study of low-lying ( $\Delta N = 1$ ) octupole excitations of the  $\beta$ -stable nucleus  ${}^{208}_{82}\text{Pb}_{126}$ , the neutron skin nucleus  ${}^{60}_{20}\text{Ca}_{40}$  and the drip line nucleus  ${}^{28}_8\text{O}_{20}$ . It can be seen that in all these nuclei, the low-lying octupole states near threshold appear as the coexistence of the collective excitations and the decoupled strong continuum strength. The properties of these low-lying states can be understood from the point of view of particle-vibration coupling.

This paper is organized as follows. The theoretical formalism of HF plus RPA calculation is described in section 2. Numerical results and discussions are shown in section 3. A summary and conclusions are given in section 4.

## 2 Formalism

The unperturbed strength function is defined by[12]

$$\begin{aligned}
 S_0 &\equiv \sum_i | \langle i | Q^\lambda | 0 \rangle |^2 \delta(E - E_i) \\
 &= \frac{1}{\pi} \text{Im} \text{Tr}(Q^{\lambda\dagger} G_0(E) Q^\lambda)
 \end{aligned}
 \tag{1}$$

while RPA strength function is given by

$$S \equiv \sum_n | \langle n | Q^\lambda | 0 \rangle |^2 \delta(E - E_n)$$

$$= \frac{1}{\pi} \text{Im} \text{Tr}(Q^{\lambda\dagger} G_{RPA}(E) Q^\lambda), \quad (2)$$

where  $G_0$  is the noninteracting p-h Green function, and  $G_{RPA}(E)$  is the RPA response function including the effect of the coupling to the continuum,

$$G_{RPA} = G_0 + G_0 v_{ph} G_{RPA} = (1 - G_0 v_{ph})^{-1} G_0. \quad (3)$$

In Eqs. (1) and (2),  $Q^\lambda$  represents one-body operators and is written as

$$Q_\mu^{\lambda=3, \tau=0} = \sum_i r_i^3 Y_{3\mu}(\hat{r}_i), \quad \text{for isoscalar octupole strength,} \quad (4)$$

$$Q_\mu^{\lambda=3, \tau=1} = \sum_i \tau_z(i) r_i^3 Y_{3\mu}(\hat{r}_i), \quad \text{for isovector octupole strength.} \quad (5)$$

The transition density for an excited state  $|n\rangle$  is defined by

$$\delta\rho_{n0}(\vec{r}) \equiv \langle n | \sum_i \delta(\vec{r} - \vec{r}_i) | 0 \rangle, \quad (6)$$

which can be obtained by RPA response function

$$\delta\rho_{n0}(\vec{r}) = \alpha \int \text{Im}[G_{RPA}(\vec{r}, \vec{r}'; E_{res})] Q^\lambda(\vec{r}') d\vec{r}', \quad (7)$$

where the normalization factor  $\alpha$  is determined from the transition strength  $S(\lambda)$  by

$$\alpha = \frac{1}{\pi \sqrt{S(\lambda)}}. \quad (8)$$

The radial transition density is defined by

$$\delta\rho_{n0}(\vec{r}) \equiv \delta\rho_\lambda(r) Y_{\lambda\mu}^*(\hat{r}). \quad (9)$$

The transition current is

$$J_{n0}(\vec{r}) = \langle n | \sum_i \frac{\hbar}{2mi} \{ \delta(\vec{r} - \vec{r}_i) \vec{\nabla}_i - \overleftarrow{\nabla}_i \delta(\vec{r} - \vec{r}_i) \} | 0 \rangle, \quad (10)$$

which can be expanded in the complete set of the vector spherical harmonics,

$$J_{n0}(\vec{r}) = (-i) \sum_{l=\lambda\pm 1} J_{\lambda l} \vec{Y}_{\lambda l, \mu}^*(\hat{r}). \quad (11)$$

The radial current component  $J_{\lambda l}$  is defined as

$$\begin{aligned} J_{\lambda l} &= i \int \vec{Y}_{\lambda, \mu}(\hat{r}) J_{n0}(r) d\hat{r} \\ &= \langle n | \sum_i \frac{\hbar}{2m} \{ \delta(r - r_i) [Y_l^*(\hat{r}_i) \times (\vec{\nabla}_i^+ - \overleftarrow{\nabla}_i^+)]_{\lambda \mu} \} | 0 \rangle. \end{aligned} \quad (12)$$

In the Bohr-Tassie model, the transition density [8,9] is

$$\delta\rho_{\lambda\tau}(r) \propto r^{\lambda-1} \frac{d\rho_0(r)}{dr}, \quad \text{for } \lambda > 0, \quad (13)$$

and the radial current components [13] are

$$J_{\lambda l} \propto \begin{cases} r^{\lambda-1} \rho_0(r), & \text{for } l = \lambda - 1, \\ 0, & \text{for } l = \lambda + 1. \end{cases} \quad (14)$$

The Tassie transition density (13) is normalized according to the following relationship

$$S(\lambda) = \left| \int \delta\rho_{\lambda\tau}(r) r^{(\lambda+2)} dr \right|^2, \quad (15)$$

where  $S(\lambda)$  is the transition strength of RPA state. This means that the normalized Tassie transition density should give the same strength as that of RPA state.

In the present work, the properties of low-lying octupole excitations are studied from particle-vibration coupling. For octupole excitation, we use the radial dependence of the particle-vibration coupling

$$V_{\text{pv}}(r) \sim r^2 \frac{dU(r)}{dr}, \quad (16)$$

or

$$V_{\text{pv}}(r) \sim r^2 \frac{d\rho_0}{dr}, \quad (17)$$

where  $U(r)$  is the HF potential and  $\rho_0(r)$  is the ground state density. Eq.(16) has been successfully used for the coupling of particle to shape oscillations in Ref.[8].

The sign of the ratio

$$\frac{\langle p|V_{\text{pv}}(r)|h \rangle}{\langle p|r^3|h \rangle} = \frac{\int \delta\rho_{ph}(r)V_{\text{pv}}(r)r^2 dr}{\int \delta\rho_{ph}(r)r^5 dr} \quad (18)$$

determines the influence of particle-vibration coupling on the strength of the unperturbed  $p - h$  excitations[14]. The magnitude of the ratio is a measure of how strongly the unperturbed strength of this  $p - h$  excitation is modified by performing RPA calculation. If the ratio is equal to zero, the unperturbed strength of this  $p - h$  transition will remain unchanged by the RPA correlation.

### 3 Results and discussions

We first perform the HF calculation with the SkM\* interaction and then use the RPA with the same interaction including simultaneously both the IS and the IV correlation. It is solved in the coordinate space with the Green's function method, taking into account the continuum exactly.

The calculated unperturbed strengths of  ${}^{208}_{82}\text{Pb}_{126}$ ,  ${}^{60}_{20}\text{Ca}_{40}$  and  ${}^{28}_8\text{O}_{20}$  are shown in Fig. 1. In the harmonic oscillator model, the low-lying octupole strength ( $\Delta N = 1$ ) is approximately equal to the high-lying ( $\Delta N = 3$ ) strength in the large  $N$  limit, and the low-lying and high-lying octupole strengths approximately exhaust 25% and 75% of the energy weighted sum rule, respectively. In real  $\beta$ -stable nuclei  $N$  is finite and the low-lying strength is less than that predicted by harmonic oscillator model in the large  $N$  limit. From Fig.1(a) it can be seen that for  ${}^{208}_{82}\text{Pb}_{126}$ , the unperturbed low-lying ( $\Delta N = 1$ ) strength is centered at about 8 MeV and spread over the same order of energy range. It exhausts approximately 40% of total strength. The high-lying ( $\Delta N = 3$ ) strength is centered at about 24 MeV and exhausts approximately 60% of total strength. For  ${}^{60}_{20}\text{Ca}_{40}$ , the unperturbed strength (see Fig.1(b)) spreads over an energy range from 2 MeV to 15 MeV and exhausts about 60% of total strength. While for  ${}^{28}_8\text{O}_{20}$  (see Fig.1(c)), except a few high-lying proton excitations, nearly all of the octupole strength lies within the low energy region. For  ${}^{60}_{20}\text{Ca}_{40}$  and  ${}^{28}_8\text{O}_{20}$ , large amount of neutron unperturbed octupole strengths are shifted down to very low energy region. This downward shifting of the octupole strengths is attributed to the disappearance of magic number  $N=50$  for  ${}^{60}_{20}\text{Ca}_{40}$  as shown in Fig.2(a), and the disappearance of magic numbers  $N=20$  and  $N=28$  for  ${}^{28}_8\text{O}_{20}$  as shown in Fig.2(b). For all the three nuclei, the calculated energy weighted sum rules are equal to the classical sum rules to a good accuracy.

In Fig.2, one-particle energies are given with fixed neutron number for (a) $N=20$  and (b) $N=40$  as a function of proton number. It is easy to see that in Fig.2(a),

when it is near the neutron drip line, the magic number  $N=20$  is disappearing, which agrees with the experimental observation[15], and new magic number  $N=16$  appears, which is consistent with the conclusion in Ref.[16]. Similar phenomena appear also in Fig.2(b). Near the neutron drip line,  $N=50$  magic number is disappearing.

Fig .3 gives the IS and IV RPA octupole strength for the  $^{208}_{82}Pb_{126}$ ,  $^{60}_{20}Ca_{40}$  and  $^{28}_8O_{20}$ . For  $\beta$ -stable nucleus  $^{208}_{82}Pb_{126}$  (Fig.3(a)), we see a strong IS peak below threshold at  $Ex=3.48$  MeV with strength  $B(\lambda = 3, IS : 3^- \rightarrow 0^+) = 5.68 \times 10^5 fm^6$ , which corresponds to  $B(E3 : 3^- \rightarrow 0^+) = (\frac{Ze}{A})^2 \times 5.68 \times 10^5 fm^6 = 0.89 \times 10^5 e^2 fm^6$ . These values are comparable to experimental data  $B(E3 : 3^- \rightarrow 0^+) = 1.0 \times 10^5 e^2 fm^6$  at energy 2.61 MeV . The IS giant resonance is at about 20.5 MeV and the IV giant resonances are mainly distributed in the energy region from 25 MeV to 35 MeV.

In Fig.4 and Fig.5 we show,for the case of  $^{208}_{82}Pb_{126}$ , the transition densities and radial current components of IS excitation at  $Ex=3.48$  MeV, IS giant resonance at  $Ex=20.5$  MeV, and IV giant resonance at  $Ex=34.2$  MeV, together with the prediction of the Bohr-Tassie model, respectively. From these figures, it can be seen that the IS and IV octupole excitations are surface modes and they are well described by the collective model. For the strong collective IS state at 3.48 MeV in Fig.4(a) and Fig.5(a), there are some difference between two models at small  $r$ , but in the surface region with  $r$  at about  $7 fm$ , this excitation can well be described by the Bohr-Tassie model.

In neutron-excess nuclei, the IS mode (shape vibration) gives rise to a IV moment which is proportional to  $(N - Z)$ , so the strength of an IS mode carries IV strength, and the ratio of IV strength/IS strength is expected to be  $(\frac{N-Z}{A})^2$  as pointed in Refs. [4,10,17]. We calculated this ratio for collective IS modes at  $Ex=3.48$  MeV and giant IS resonance around  $Ex=20.5$  MeV in  $^{208}_{82}Pb_{126}$ . Both modes give the ratios  $(\frac{126-82}{208})^2$  to a good accuracy.

For  $^{60}_{20}Ca_{40}$  (Fig.3(b)), the main IS strengths are shifted down to low energy region. Below 5 MeV there are 4 strong IS peaks and one of them is below threshold ( $Ex=1.91$  MeV). From the transition densities and radial current components in Fig.6, the IS collective state at  $Ex=1.91$  MeV can be described by the Bohr-Tassie model. The transition densities and radial current components of the other three IS peaks below 5 MeV are shown in Fig.7 and Fig.8, respectively. From Fig.7 it can be seen that these three IS peaks are surface modes and both neutrons and protons contribute. This indicates they are collective. In the central region of the nucleus there are differences between the transition densities of the Bohr-Tassie model and those of RPA calculation. But in the surface region the results of RPA calculation are similar to those of collective model. From Fig.8 we see that for the currents, the Bohr-Tassie model results differ from the ones from RPA substantially, even in the surface

region. For example, in our RPA calculation the small component  $j_{3,4}(r)$  is comparable to the large component  $j_{3,2}(r)$ , but the Bohr-Tassie model gives  $j_{3,4}(r) = 0$ . This difference will be explained from the viewpoint of particle-vibration coupling later.

The ratios of IV strength/IS strength for these 4 strong IS peaks (below 5 MeV in  ${}^{60}_{20}\text{Ca}_{40}$ ) are also calculated. We find that, however, unlike the case in  $\beta$ -stable nucleus  ${}^{208}_{82}\text{Pb}_{126}$ , the calculated ratios are larger than  $(\frac{N-Z}{A})^2$  by factor 2 to 4. This result is closely related to the neutron orbits of small binding energies and they push down the unperturbed octupole strengths to very low energy region.

For  ${}^{28}_8\text{O}_{20}$  (see Fig.3(c)), the high-lying IS giant resonance nearly disappears and almost all the IS octupole strengths are shifted down to low energy. The transition densities and radial current components for the lowest three peaks are shown in Fig.9 and Fig.10, respectively. From Fig.9 we see that the three peaks are surface modes and both protons and neutrons contribute. In Fig.1 and Fig.3 we notice that the IS strengths of these peaks are larger than those of unperturbed ones, which shows they are collective. The Bohr-Tassie model can approximately describe the transition densities in the surface region. The Bohr-Tassie model gives quite different currents properties for these IS peaks in Fig.10. The reason will be analyzed later.

We also calculated the ratios of IV strength/IS strength for these three IS peaks. The calculated values are factor 3 to 5 larger than  $(\frac{N-Z}{A})^2$  in  ${}^{28}_8\text{O}_{20}$ . Similar to  ${}^{60}_{20}\text{Ca}_{40}$ , this is also related to the least bound neutrons.

Next we try to understand the collective properties of these low-lying IS excitations in  ${}^{60}_{20}\text{Ca}_{40}$  and  ${}^{28}_8\text{O}_{20}$  based on the particle-vibration coupling. We have checked that the signs of the ratio Eq. (18) in our cases are always positive, so we only consider their absolute values here. Fig.11 shows a few low-lying neutron unperturbed octupole strengths in  ${}^{60}_{20}\text{Ca}_{40}$  for radial operators  $r^3$ ,  $r^2\frac{dU(r)}{dr}$  and  $r^2\frac{d\rho_0(r)}{dr}$ , and Fig.12 shows the corresponding quantities for  ${}^{28}_8\text{O}_{20}$ . Here where  $U(r)$  is the neutron radial HF potential and  $\rho_0(r)$  is the ground state density. From Fig.11 we see that for the transition from bound state to non-resonance state,  $1f_{\frac{5}{2}} \rightarrow 3s_{\frac{1}{2}}$ , there is a pronounced peak in octupole strength function for radial operator  $r^3$ , but almost no peaks for the other two radial operators  $r^2\frac{dU(r)}{dr}$  and  $r^2\frac{d\rho_0(r)}{dr}$ , respectively. Just like the transitions from bound states to bound states,  $1f_{\frac{5}{2}} \rightarrow 1g_{\frac{3}{2}}$  and  $2p_{\frac{3}{2}} \rightarrow 1g_{\frac{3}{2}}$ , there are strong peaks of octupole strengths for all three radial operators in corresponding energy region for the transitions from bound states to resonance states,  $1f_{\frac{5}{2}} \rightarrow 2d_{\frac{5}{2}}$  and  $2p_{\frac{1}{2}} \rightarrow 2d_{\frac{5}{2}}$ . It means that the ratios Eq. (18) for transitions to nonresonance states are much smaller than those for the transitions to resonance states and to bound states. In RPA calculation the unperturbed octupole strength of the radial operator  $r^3$  for the transition from bound state to nonresonance state

$1f_{\frac{5}{2}} \rightarrow 3s_{\frac{1}{2}}$  will hardly be affected, but the strengths of the radial operator  $r^3$  for the transitions from bound states to resonance states and to bound states will be strongly absorbed into the collective excitations. Because the unperturbed octupole strength of the transition from bound state to nonresonance state  $1f_{\frac{5}{2}} \rightarrow 3s_{\frac{1}{2}}$  for radial operator  $r^3$  is mainly distributed within the energy region from 3.0 MeV to 4.5 MeV, there is the coexistence of the collective excitations and the decoupled strong continuum strength near the threshold in these three lowest IS peaks. That is why the Bohr-Tassie model can only well describe the transition density of RPA calculation in the surface region for the low-lying excitations in  ${}^{60}_{20}\text{Ca}_{40}$ , but it can not well describe the calculated transition current.

From Fig.12 we see similar results for  ${}^{28}_8\text{O}_{20}$ . For transition from bound state to nonresonance state,  $1d_{\frac{3}{2}} \rightarrow 2p_{\frac{3}{2}}$ , the ratio in Eq. (18) is much smaller than those for transitions from bound states to resonance states,  $1d_{3/2} \rightarrow 1f_{7/2}$  and  $2s_{1/2} \rightarrow 1f_{7/2}$ . In these three lowest IS peaks, there is the coexistence of the collective excitations and the decoupled strong continuum strength near the threshold. That is the reason why the Bohr-Tassie model can only approximately describe the calculated transition density in the surface region for the three lowest IS peaks in  ${}^{28}_8\text{O}_{20}$ , but it can not well describe the transition current of our calculation.

## 4 Summary and Conclusions

The octupole vibrations for the  $\beta$ -stable nucleus  ${}^{208}_{82}\text{Pb}_{126}$ , the neutron skin nucleus  ${}^{60}_{20}\text{Ca}_{40}$  and the drip line nucleus  ${}^{28}_8\text{O}_{20}$  are studied. It is found that the lowest IS excitation below threshold for the nuclei  ${}^{208}_{82}\text{Pb}_{126}$  and  ${}^{60}_{20}\text{Ca}_{40}$ , and IS and IV giant resonances of the  $\beta$ -stable nucleus  ${}^{208}_{82}\text{Pb}_{126}$  can be well described by collective model, at least in the surface region.

For the neutron skin nucleus  ${}^{60}_{20}\text{Ca}_{40}$  and the neutron drip line nucleus  ${}^{28}_8\text{O}_{20}$ , there exist strengths of transitions from bound states to bound states, resonance states, and nonresonance states in the low-lying unperturbed neutron octupole strength ( $\Delta N = 1$ ). The strengths of transitions to nonresonance states are nearly unaffected and the strengths of other transitions are strongly absorbed into collective states by taking into account the RPA correlation. So there is the coexistence of the collective excitations and the decoupled strong continuum strength near the threshold in the lowest IS states.

We also find that, for the  $\beta$ -stable nucleus  ${}^{208}_{82}\text{Pb}_{126}$ , both low-lying IS states and giant IS resonances carry IV component and the ratios of IV strength/IS strength are equal to  $(\frac{N-Z}{A})^2$  to good accuracy, but for the neutron skin nucleus  ${}^{60}_{20}\text{Ca}_{40}$  and the neutron drip line nucleus  ${}^{28}_8\text{O}_{20}$ , these ratios for a few



lowest strong IS excitations are much larger than  $(\frac{N-Z}{A})^2$ . These results are closely related to the small binding energies of neutron orbits in these nuclei. The octupole transitions from these orbits are mainly distributed in low energy region, so the contribution to low-lying ( $\Delta N = 1$ ) octupole states from neutrons are much larger than those from protons.

This work is supported by the National Natural Science Foundation of China under contact 10047001 and the Major State Basic Research Development Program under contract No. G200077400. We are grateful to I. Hamamoto and H. Sagawa for providing us with continuum RPA program.

## References

- [1] I. Hamamoto, H. Sagawa and X. Z. Zhang, Phys. Rev. C 53 (1996) 765.
- [2] I. Hamamoto and H. Sagawa, Phys. Rev. C 53 (1996) R1492.
- [3] I. Hamamoto and H. Sagawa, Phys. Rev. C 54 (1996) 2369.
- [4] I. Hamamoto, H. Sagawa and X. Z. Zhang, Phys. Rev. C 55 (1997) 2361; J. Phys. G 24 (1998) 1417.
- [5] I. Hamamoto, H. Sagawa and X. Z. Zhang, Nucl. Phys. A 626 (1997) 669.
- [6] I. Hamamoto, H. Sagawa and X. Z. Zhang, Phys. Rev. C 56 (1997) 3121.
- [7] I. Hamamoto, H. Sagawa and X. Z. Zhang, Phys. Rev. C 57 (1998) R1064.
- [8] A. Bohr and B. R. Mottelson, Nuclear Structure, Vol. II (Benjamin, New York, 1975).
- [9] L. T. Tassie, Australian, J. Phys. 9 (1956) 407.
- [10] F. Catara, E. G. Lanza, M. A. Nagarajan, and A. Vitturi, Nucl. Phys. A 614 (1997) 86.
- [11] I. Hamamoto, H. Sagawa and X. Z. Zhang, Phys. Rev. C 64 (2001) 024313.
- [12] I. Hamamoto, H. Sagawa and X. Z. Zhang, Nucl. Phys. A 648 (1999) 203.
- [13] T. Suzuki and D. J. Rowe, Nucl. Phys. A 286 (1977) 307.
- [14] I. Hamamoto and X. Z. Zhang, Phys. Rev. C 58 (1998) 3388.
- [15] D. Guillemaud-Mueller, *et al.*, Nucl. Phys. A 426 (1984) 37; T. Motobayashi, *et al.*, Phys. Lett. B 346 (1995) 9.
- [16] A. Ozawa, T. Kobayashi, Y. Suzuki, K. Yashida and I. Tanihata, Phys. Rev. Lett. 84 (2000) 5439.
- [17] H. Sagawa, Phys. Rev. C 64 (2002) 064314.

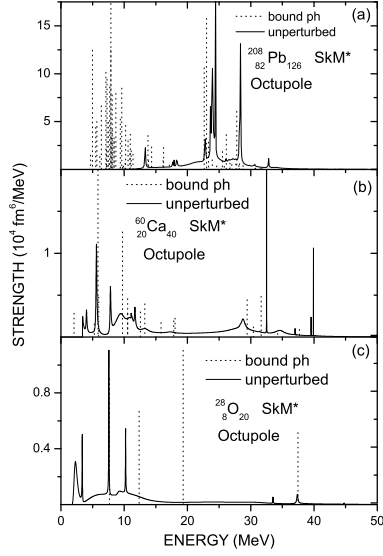


Fig. 1. Unperturbed octupole strengths of (a)  $^{208}_{82}\text{Pb}_{126}$ , (b)  $^{60}_{20}\text{Ca}_{40}$  and (c)  $^{28}_8\text{O}_{20}$ .

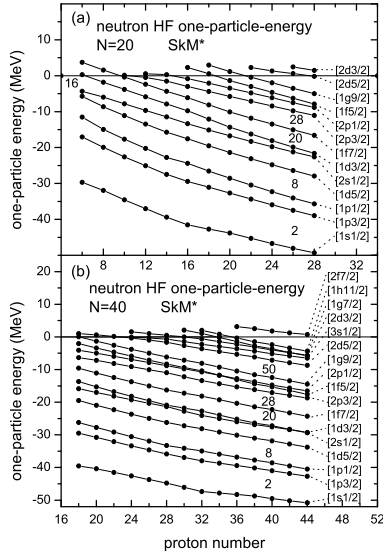


Fig. 2. One-particle energies vary with proton number for (a) neutron number  $N = 20$  and (b) neutron number  $N = 40$ .

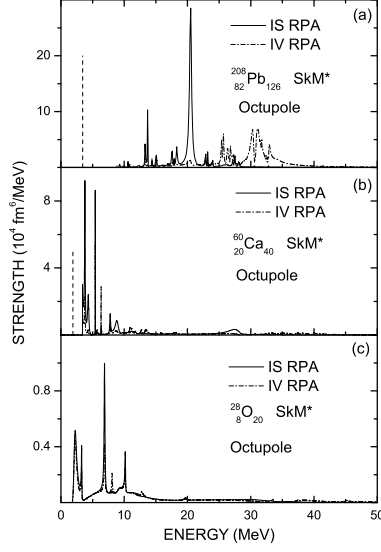


Fig. 3. Isoscalar and isovector octupole strengths of (a)  $^{208}_{82}\text{Pb}_{126}$ , (b)  $^{60}_{20}\text{Ca}_{40}$  and (c)  $^{28}_8\text{O}_{20}$ .

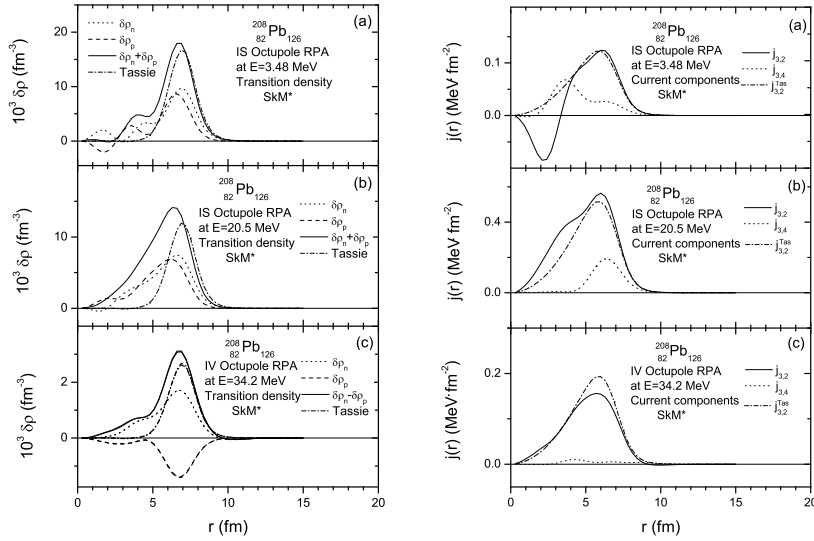


Fig. 4. (left) Radial transition densities of low-lying and high-lying IS and IV octupole modes of  $^{208}_{82}\text{Pb}_{126}$ .

Fig. 5. (right) Radial transition current components of low-lying and high-lying IS and IV octupole modes of  $^{208}_{82}\text{Pb}_{126}$ .

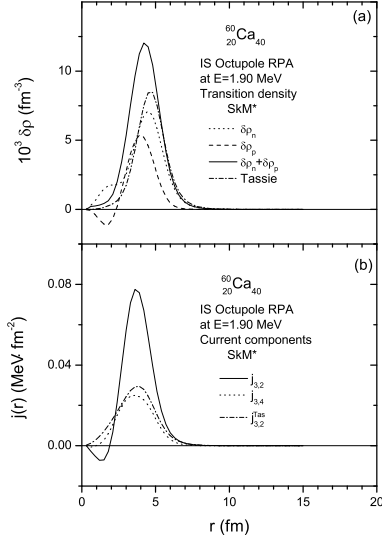


Fig. 6. Radial transition densities and current components of low-lying IS octupole modes of  $^{60}_{20}\text{Ca}_{40}$ .

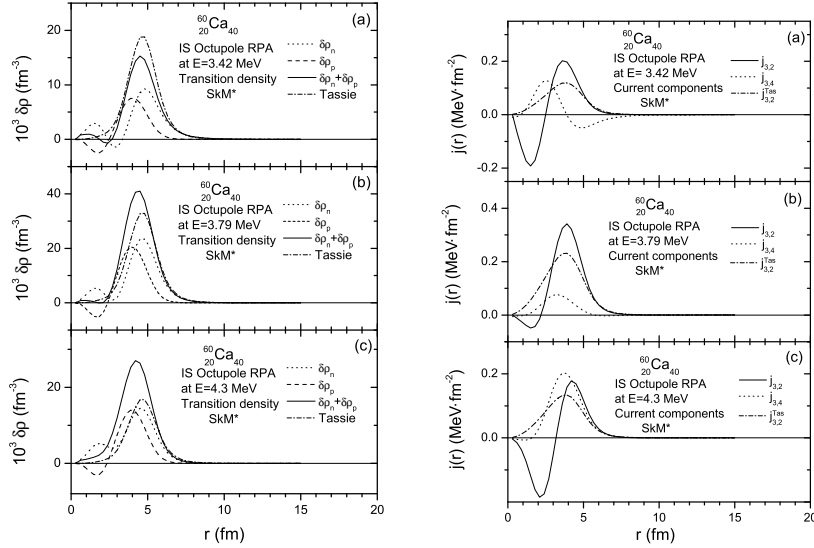


Fig. 7. (left) Radial transition densities of low-lying IS octupole modes of  $^{60}_{20}\text{Ca}_{40}$ .

Fig. 8. (right) Radial current components of low-lying IS octupole modes of  $^{60}_{20}\text{Ca}_{40}$ .

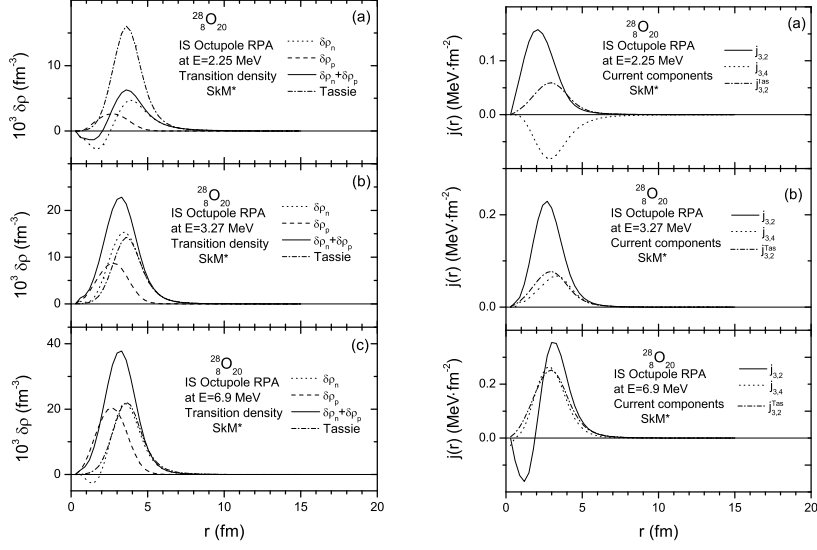


Fig. 9. (left) Radial transition densities of low-lying IS octupole modes of  ${}^{28}_8\text{O}_{20}$ .

Fig. 10. (right) Radial current components of low-lying IS octupole modes of  ${}^{28}_8\text{O}_{20}$ .

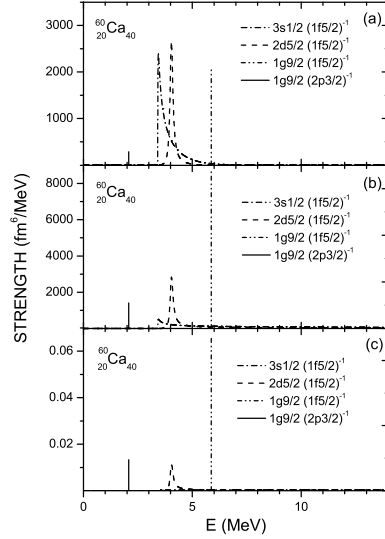


Fig. 11. Few low-lying unperturbed octupole strength in  ${}^{60}_{20}\text{Ca}_{40}$  for radial operators (a)  $r^3$ , (b)  $r^2 \frac{dU(r)}{dr}$  and (c)  $r^2 \frac{d\rho_0(r)}{dr}$ , where  $U(r)$  is the neutron radial HF potential and  $\rho_0(r)$  is the ground state density.

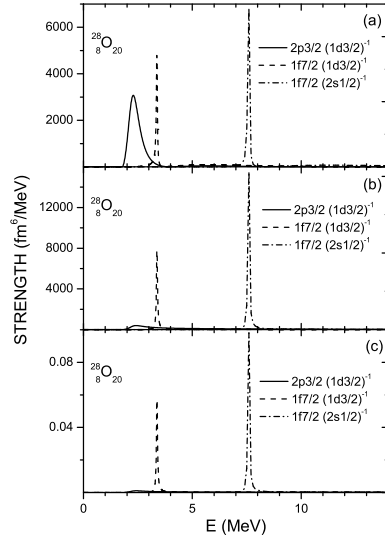


Fig. 12. Few low-lying unperturbed octupole strength in  ${}^{28}\text{O}_{20}$  for radial operators (a)  $r^3$ , (b)  $r^2 \frac{dU(r)}{dr}$  and (c)  $r^2 \frac{d\rho_0(r)}{dr}$ , where  $U(r)$  is the neutron radial HF potential and  $\rho_0(r)$  is the ground state density.